

Emergence of quasiparticle Bloch states in artificial crystals crafted atom-by-atom

J. Girovsky¹, J. L. Lado², F. E. Kalff¹, E. Fahrenfort¹, L.J.J.M. Peters¹, J. Fernández-Rossier^{2,3} and A. F. Otte^{1*}

¹Department of Quantum Nanoscience, Kavli Institute of Nanoscience, Delft University of Technology, Lorentzweg 1, 2628 CJ Delft, The Netherlands.

² QuantaLab, International Iberian Nanotechnology Laboratory (INL), Avenida Mestre José Veiga, 4715-310 Braga, Portugal.

³Departamento de Física Aplicada, Universidad de Alicante, San Vicente del Raspeig, 03690 Spain.

*Corresponding author: a.f.otte@tudelft.nl

The interaction of electrons with a periodic potential of atoms in crystalline solids gives rise to band structure. The band structure of existing materials can be measured by photoemission spectroscopy and accurately understood in terms of the tight-binding model, however not many experimental approaches exist that allow to tailor artificial crystal lattices using a bottom-up approach. The ability to engineer and study atomically crafted designer materials by scanning tunnelling microscopy and spectroscopy (STM/STS) helps to understand the emergence of material properties. Here, we use atom manipulation of individual vacancies in a chlorine monolayer on Cu(100) to construct one- and two-dimensional structures of various densities and sizes. Local STS measurements reveal the emergence of quasiparticle bands, evidenced by standing Bloch waves, with tuneable dispersion. The experimental data are understood in terms of a tight-binding model combined with an additional broadening term that allows an estimation of the coupling to the underlying substrate.

Atom manipulation by means of STM is a viable way of constructing atomically precise artificial structures¹. Among others, the technique can be used to engineer atomic scale logic devices^{2,3}, low dimensional magnetic systems^{4,5,6} or atomic data storages^{7,8,9}. As our abilities to manipulate atoms on a large scale are improving, the formation of atomically designed artificial crystals becomes of particular interest driven by a demand for new materials where the properties are defined by emerging quasiparticle states¹⁰. Common approaches to build low-dimensional artificial materials by STM include confinement of electronic surface states through precise assembly of individual atoms and/or molecules^{11,12,13} self-assembly of molecular networks^{14,15}, and manipulation of dangling bonds¹⁶ or surface vacancies¹⁷. The recent development of large-scale fully automated placement of atomic vacancies on a chlorinated copper crystal surface⁹ provides an excellent platform to explore various lattice composition. These vacancies were found to host a localized vacancy state in the surface band gap, similar to dopants in semiconductors, allowing their combined electronic states to be modelled by means of tight-binding approximation¹⁸.

Here, we present a study of artificial one- and two-dimensional structures built from Cl vacancies in an otherwise perfect monolayer square lattice formed by chlorine atoms on a Cu(100) surface. Using

local electron tunnelling spectroscopy, we demonstrate that we are able to reach system scales where the spectral properties no longer depend on size and which can therefore be considered to be in the bulk limit. For structures with a sufficiently large vacancy density, we observe quasiparticle Bloch waves that can be simulated by using a tight-binding model. Analysis of the Bloch wave dispersion allows us to extract quasiparticle effective masses, which are found to depend strongly on the chosen lattice structure.

A monolayer of chlorine atoms on Cu(100) exhibits a surface band gap E_g of about 7 eV (see inset of Fig. 1a) as well as a shift in the substrate's work function by 1.35 eV¹⁹, suggesting a significant charge transfer between the substrate and chlorine atoms and formation of the interface dipole moment²⁰. Theoretical calculations predict a charge of 0.5 electron accumulated on chlorine atoms and depletion of density of states (DOS) at the top most layer of the copper substrate²¹. Other materials with a similarly large surface band gap, e.g. Cu₂N on Cu(100) ($E_g \sim 4$ eV)²², NaCl bilayers on copper substrates ($E_g \sim 8.5$ eV)²³, and non-polar MgO films on Ag(100) ($E_g \sim 6$ eV)²⁴, have found applications in studies of elementary excitations in individual molecules and/or adatoms^{3,25,26,27}. Formation of an insulating monolayer at metal substrates has little effect on the valence band maximum, however significantly affects the conduction band minimum, which was found as high as ~ 4 eV for NaCl bi- and tri-layers on the copper substrates²³. In our case, a sharp step at ~ 3.5 V denotes the conduction band minimum (black curve Fig. 1a) with a very low DOS below the threshold.

When the Cl/Cu(100) interface possesses defects in the form of missing chlorine atoms (dark square in the inset of Fig. 1a), a localized electronic vacancy state (VS) is resolved at lower voltages ~ 3.4 V (green curve Fig. 1a). The occurrence of this VS shows similarities to the localized state in the gap region of hydrogen-doped Si(100) surfaces¹⁶ or that of a chlorine vacancy in the NaCl/Cu(111) system²³. When two chlorine vacancies are brought close to each other, by means of atom manipulation, the spatial overlap of their vacancy state wave functions leads to the formation of a pair of bonding and anti-bonding orbitals¹⁸. These molecular orbitals can be effectively described within the tight-binding model and their energy depends on the hopping term t – a measure of the overlap of the two VS.

We built chains of the Cl/Cu(100) vacancies of various lengths L and lattice spacing ($\{0,3\}$, $\{0,2\}$ and $\{1,1\}$) as shown in Fig. 1. Differential conductance (dI/dV) spectra were acquired along chains of length $L = 16$, (L - number of vacancy sites), for all three spacing parameters. The spectra reveal a shift of the conductance band minimum toward lower voltages and broadening of the spectral features for the lattice of smaller spacing. Both the shift and the band broadening result from the increased overlap between neighbouring sites. The observed spectral features show a correlation with the position within the chains, i.e. the band minimum measured on outer vacancies is found at higher energies compared to that resolved on inner ones. This dependence is further corroborated for edge vacancies within denser lattices where the effect is more pronounced (e.g. Fig. 1e). Spectra acquired on the chains' chlorine atoms rather than the vacancies show a similar spatial dependence of the band onset.

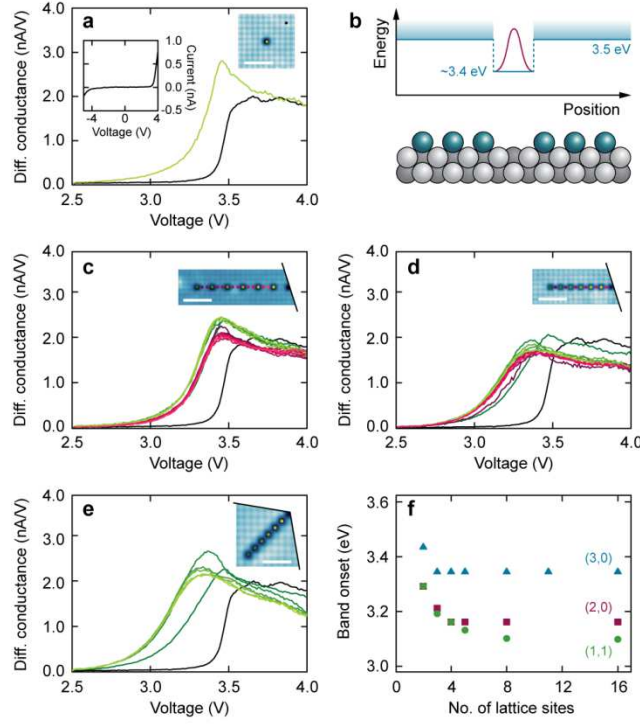


Figure 1 | Differential conductance spectra acquired on chlorine vacancy in Cl/Cu(100) substrate and in artificial 1D lattices crafted from the vacancies. a, dI/dV measurement taken inside a chlorine vacancy (green) and on the bare Cl/Cu(100) substrate (black). Dots depict positions where spectra were taken. The inset shows an I - V curve acquired from -4.5 to 4.0 V where the surface band gap of $E_g \sim 7$ eV is clearly visible. **b,** Sketch denoting the energy level of the vacancy state with respect to the band continuum. **c, d, e,** dI/dV spectra taken on vacancy sites and/or chlorine interstices (locations indicated by coloured dots in the insets) on lattices with 16 vacancy sites for spacing configurations $\{0,3\}$ (c), $\{0,2\}$ (d) and $\{1,1\}$ (e). **f,** Evolution of the band onset as a function of lattice spacing and lattice size. Data points indicate the position of the band onset extracted from spectra taken on the middle vacancy of each lattice. In the case of an even-length chain, the averaged value measured on the two centre vacancies is shown. STM images were acquired in constant current mode $I = 2$ nA and $V = 500$ mV. All scale bars are 2 nm.

In Fig. 1f we plot the dependence of the band onset as a function of the chain length L , measured at the centre of each chain. For each lattice spacing, the band onset is found to saturate, however at different values of L : the $\{0,3\}$ chains saturate at 3.35 eV already for $L = 3$, the $\{0,2\}$ chains at 3.18 eV for $L = 5$ and the $\{1,1\}$ chains at 3.1 eV for $L = 8$. The saturation of the band minimum implies an approach of the limit where edge effects no longer play a role for the inner vacancies and the chains can effectively be considered of infinite length. Furthermore, the observed shift relates to the size of the hopping parameter t which increases for shorter lattice spacing¹⁸.

To further investigate the band formation, we built two-dimensional structures with varying lattice spacing, $\{3,3\}$, $\{2,3\}$, $\{2,2\}$ as well as ‘stripes’ and ‘checkerboard’ arrays, all of varying lattice size (Fig. 2). Moving inward along the diagonal of each structure, the position of the band onset shifts towards lower energies for denser and larger lattices, similar to the 1D chains. In the case of the stripe phase we observe two band onsets, $E_1 = 2.8$ eV and $E_2 = 3.1$ eV, measured at the centre vacancy (see Fig. 2g). We attribute these to the two different lattice constants along the lattice diagonals, $a_1 = 0.51$ nm and $a_2 = 0.69$ nm. Assuming that the hopping parameter is exponentially dependent on the distance¹⁸ and the bandwidth is linearly proportional to the hopping parameter t , the band is expected to be symmetric around the energy $E = 3.4$ eV of a single vacancy. We estimate

the widths of the respective bands to be $W_1 = 1.2$ eV and $W_2 = 0.6$ eV, leading to a ratio $W_1/W_2 \sim 2$. This ratio is somewhat higher than the ratio between the hopping parameters $t(a_1)/t(a_2) \sim 1.2$, suggesting that another effect may play a role, affecting the width and/or position of the band, e.g. an electric field due to positively charged neighbouring vacancies observed at polar insulating surfaces. Such an electric field can cause a shift of the band onset towards lower energies, which is expected to be larger for denser lattices¹⁷.

The checkerboard lattice (Fig. 2e) was found to be more sensitive to relatively high tunnelling currents than lattices with lower vacancy coverage. For large tunnelling current and voltage values (e.g. > 2 nA at ~ 4.7 V), we observed chlorine atoms changing their position, rendering the structure unstable. For this reason, instead of acquiring dI/dV spectra, we measured the dependence of the tip-sample distance z as a function of sample voltage in constant current mode, i.e. dz/dV curves, that qualitatively resemble the normalized differential conductance $dI/dV \cdot V/I$ (Supplementary Figure 1).

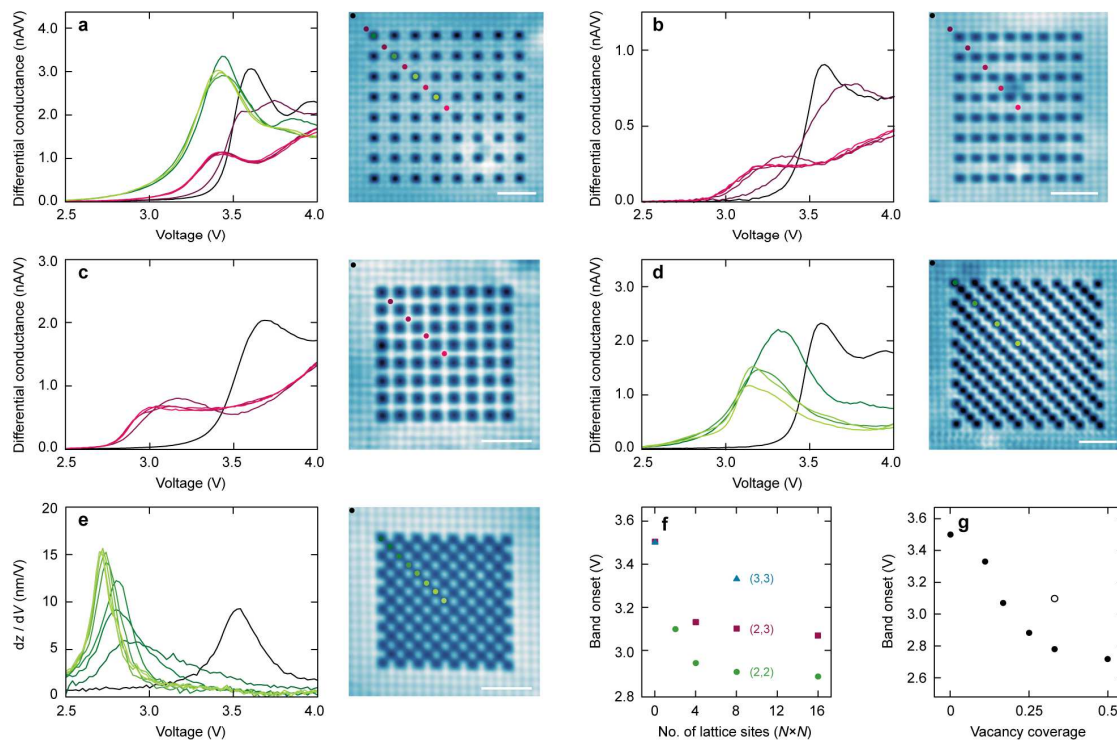


Figure 2 | Analysis of artificial 2D lattices by chlorine vacancies of Cl/Cu(100). **a, b, c, d, e,** Differential conductance spectra measured along diagonals of the lattices with spacing $\{3,3\}$ (a), $\{2,3\}$ (b), $\{2,2\}$ (c) and with stripes (d) and checkerboard (e) patterns. Coloured dots denote the positions where the spectra were acquired. **f,** Evolution of band onset as function of lattice spacing and lattice size. Band onset was extracted from the spectra taken in the middle of the lattices. **g,** Band onset as a function of lattice density, i.e. number of vacancies per unit cell. STM images were acquired in constant current mode $I = 2$ nA and $V = 500$ mV. All scale bars 2 nm.

Apart from preserving the lattice integrity, the dz/dV measurement mode also provides sufficient sensitivity to detect standing wave modes in some of the lattices that are not visible in dI/dV mode (see Methods for details). Fig. 3 shows dz/dV maps acquired on the stripe and checkerboard lattices. Interestingly, the modes are resolved very symmetric in the x and y direction, i.e. the number of

protrusions in both directions is equivalent, even though the unit cell of the stripes lattice is highly asymmetric.

To shine more light onto the standing wave pattern, we performed numerical calculations of artificial lattices of size $L \times L$ using tight-binding approach that effectively simulate dz/dV maps, which are proportional to the density of states (DOS, see Supplementary Note 1 for details). In the simplest picture, the observed modes would correspond to wave functions with two distinguished k -vectors $k_x = N\pi/L$ and $k_y = M\pi/L$. The experimentally observed modes resemble some of the calculated modes with $N = M$ (Supplementary Figure 2). However, the experimental data show a richer structure with the links connecting the very bright protrusions along x and y direction. Furthermore, the experimentally observed modes are gradually transforming from one mode to another with an increasing number of lobes. At certain energies the lobes are not spherical, but rather have an elongated shape, that splits into two with increasing voltage.

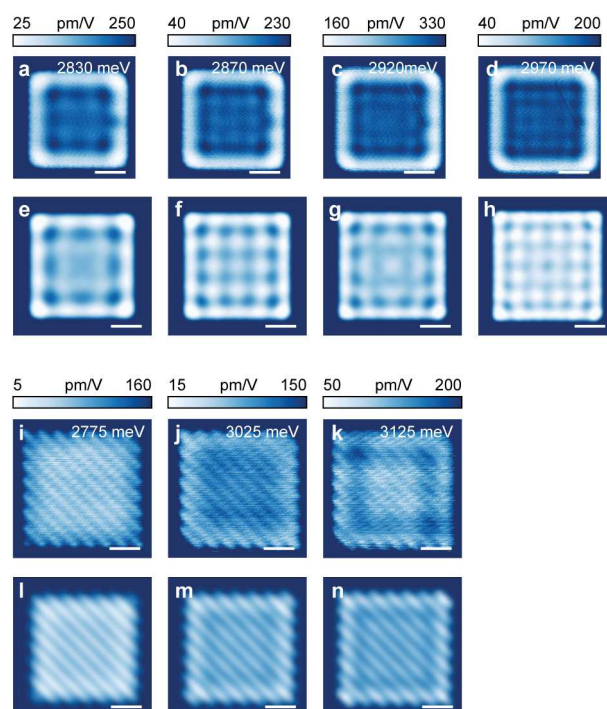


Figure 3 | dz/dV maps acquired on checkerboard and stripe lattices. **a, b, c, d**, dz/dV maps taken on an 8×8 checkerboard lattice at different energies. **e, f, g, h**, Corresponding numerical calculations using a tight-binding model including an additional hybridization term. **i, j, k, and l, m, n**, Similar as (a–d) and (e–h) for an 8×8 stripes lattice. All scale bars 2 nm.

The apparent lack of $N \neq M$ modes in our experimental data can be understood in terms of coupling of the confined modes to electronic bath underneath, mathematically represented by a self-energy with finite imaginary part. This interaction thus leads to a finite lifetime of the states and a broadening of the spectral function, which consequently overlap with neighbouring states and alter the appearance of the modes (see Methods for details on the numerical calculations). The addition of this hybridization term yields a DOS profile composed from the mixture of many individual modes that can no longer be resolved, and resembles up to very fine details the experimental STM maps, including the smooth crossover (Figs. 3e–h, l–m). Similar broadening of the energy modes was also attributed to strong electron-phonon coupling²³. As such, the experimental modes have to be

understood as coming from the mixture of many individual modes due to the finite coupling of the lattice to the underlying copper, so that at a particular energy we do not observe a single confined mode, but a weighted mixture of the neighbouring modes.

In a similar manner, we calculated the DOS on the stripe lattice, where the distance between vacancies along two lattice directions is not equal. We included two different hopping terms in our calculations in order to properly reproduce the experimental data. If only the hopping term along the direction of the stripes is considered, the numerically resolved modes within the chains are decoupled from each other and do not reflect the experimentally observed patterns (Supplementary Figure 3). Comparison of numerical results with the experimental images allows to directly extract the effective hopping parameters for the effective square lattices. In our numerical simulations we used a model with only first neighbour hopping term of -215 meV, that reproduces the features of checkerboard lattice very well, but fail to capture the features of stripe lattice. However, the tight binding model with first and second neighbour hopping parameters -139 meV and -38 meV, respectively, can reproduce both the checkerboard and stripes lattice patterns to a great extent.

The previous discussion requires investigation of the numerical and experimental dz/dV maps one by one and identify the interference patterns. The emergence of dispersive modes within the maps can be explored systematically using the quantitative fast Fourier transform (FFT) analysis of these dz/dV maps images (Figs. 4a-d). In the following, we calculate the expectation value of the square of the k -vector $\langle k^2 \rangle$ of each FFT image, thus assigning a single value to a complete dz/dV map. Plotting the energy E (aka applied bias voltage) as a function of $\langle k^2 \rangle$ we provide a dispersion curve that allows to systematically identify the energy regions where an interference pattern is visible. Fig. 4e shows the obtained dispersion diagrams for the checkerboard in the energy interval 2750 meV to 3140 meV, and for the stripes lattice in the energy interval 2775 meV to 3175 meV. The full E vs. $\langle k^2 \rangle$ plots are shown in Fig 4e.

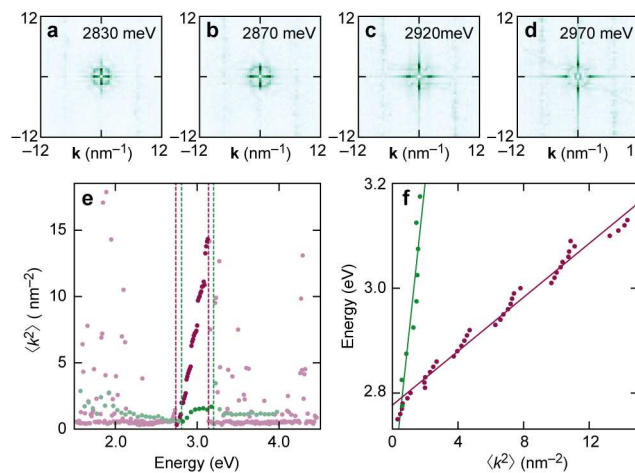


Figure 4 | Fourier analysis of the dz/dV maps. **a, b, c, d**, Evolution of the Fourier map for the checkerboard lattice at different energies, corresponding to dz/dV maps presented in Figs. 3a, b, c and d, respectively. Increasing energy leads to a shift of the maximal intensity towards higher k -vector values. **e**, Evolution of the expectation value of the square of the momentum vs. the energy for checkerboard (purple) and stripes lattice (green) in a wide energy range. Dashed lines define the energy intervals within which the dispersive modes are observed in each lattice. **f**, Dispersion plots E vs. $\langle k^2 \rangle$ for the energy intervals marked in (e). Solid lines show linear fits, from which the effective masses are extracted.

By performing linear fits to the E vs. $\langle k^2 \rangle$ plots we extract effective electron masses $m_{\text{eff}} = 1.470 \pm 0.034 m_e$ for the checkerboard and $m_{\text{eff}} = 0.131 \pm 0.025 m_e$ for the stripes lattice, where m_e is the free electron mass. The obtained values indicate that quasiparticle waves in the checkerboard lattice are heavier and therefore less mobile than those in the stripes lattice. This is in apparent contradiction to parameter values obtained from the tight binding model. Intuitively, one would expect the checkerboard lattice, being denser than the stripes lattice, to provide higher electron mobility due to larger hopping parameters, and therefore to yield a lower effective mass. The dispersive properties found from the analysis in Fig. 4 should therefore be considered as phenomenological only.

Conclusion

Engineering artificial lattices by means of atom manipulation of chlorine vacancies in the Cl/Cu(100) substrate demonstrate a way to craft artificial one- and two-dimensional materials with tuneable electronic properties. We explore the emergent band formation as we build lattices of varying structure, density and size. For all lattices studied, the bottom of the emerging band is found to shift towards lower energies, in accordance to the tight-binding model, as the lattice size or density is increased. Furthermore, we find that the band onset saturates for larger structures, implying that the effect of finite size can be neglected. In the case of two-dimensional checkerboard- and stripe-shaped lattices, we observe standing Bloch waves. These patterns are well explained using a tight-binding model that includes coupling to the electron bath. Surprisingly, the effective mass of the observed Bloch waves is found to depend strongly on the lattice geometry. Our work provides a testing ground for future designer materials where the electronic properties can be defined a priori.

References:

1. Strosio, J. A. & Eigler, D. M. Atomic and Molecular Manipulation with the Scanning Tunnelling Microscope. *Science* **254**, 1319–1326 (1991).
2. Heinrich, A. J. *et al.* Molecule Cascades. *Science* **298**, 1381–1387 (2002).
3. Khajetoorians, A. A., Wiebe, J., Chilian, B. & Wiesendanger, R. Realizing All-Spin-Based Logic Operations Atom by Atom. *Science* **332**, 1062–1064 (2011).
4. Hirjibehedin, C. F. *et al.* Spin Coupling in Engineered Atomic Structures. *Science* **312**, 1021–1024 (2006).
5. Toskovic, R. *et al.* Atomic spin-chain realization of a model for quantum criticality. *Nat. Phys.* **12**, 656–660 (2016).
6. Spinelli, A., Bryant, B., Delgado, F., Fernández-Rossier, J. & Otte, A. F. Imaging of spin waves in atomically designed nanomagnets. *Nat. Mater.* **13**, 782–785 (2014).
7. Loth, S., Baumann, S., Lutz, C. P., Eigler, D. M. & Heinrich, A. J. Bistability in Atomic-Scale Antiferromagnets. *Science* **335**, 196–199 (2012).
8. Khajetoorians, A. A. *et al.* Current-Driven Spin Dynamics of Artificially Constructed Quantum Magnets. *Science* **339**, 55–59 (2013).

9. Kalff, F. E. *et al.* A kilobyte rewritable atomic memory. *Nat. Nanotechnol.* **11**, 926–929 (2016).
10. Venema, L. *et al.* The quasiparticle zoo. *Nat. Phys.* **12**, 1085–1089 (2016).
11. Gomes, K. K., Mar, W., Ko, W., Guinea, F. & Manoharan, H. C. Designer Dirac fermions and topological phases in molecular graphene. *Nature* **483**, 306–310 (2012).
12. Pennec, Y. *et al.* Supramolecular gratings for tuneable confinement of electrons on metal surfaces. *Nat. Nanotechnol.* **2**, 99–103 (2007).
13. Slot, M. R. *et al.* Experimental realization and characterization of an electronic Lieb lattice. *eprint ArXiv: 1611.04641v1* (2016).
14. Lobo-Checa, J. *et al.* Band Formation from Coupled Quantum Dots Formed by a Nanoporous Network on a Copper Surface. *Science* **325**, 300–303 (2009).
15. Klappenberger, F. *et al.* Dichotomous Array of Chiral Quantum Corrals by a Self-Assembled Nanoporous Kagomé Network. *Nano Lett.* **9**, 3509–3514 (2009).
16. Schofield, S. R. *et al.* Quantum engineering at the silicon surface using dangling bonds. *Nat. Commun.* **4**, 1649 (2013).
17. Schuler, B. *et al.* Effect of electron-phonon interaction on the formation of one-dimensional electronic states in coupled Cl vacancies. *Phys. Rev. B* **91**, 235443 (2015).
18. Drost, R., Ojanen, T., Harju, A. & Liljeroth, P. Topological states in engineered atomic lattices. *eprint ArXiv: 1611.01049v2* (2016).
19. Nowakowski, J. *et al.* Probing the Reactivity of Functionalized Surfaces by Porphyrin Metalation. *ChemistrySelect* **1**, 891–895 (2016).
20. Roman, T. & Groß, A. Periodic Density-Functional Calculations on Work-Function Change Induced by Adsorption of Halogens on Cu(111). *Phys. Rev. Lett.* **110**, 156804 (2013).
21. Migani, A. & Illas, F. A Systematic Study of the Structure and Bonding of Halogens on Low-Index Transition Metal Surfaces. *J. Phys. Chem. B* **110**, 11894–11906 (2006).
22. Ruggiero, C. D., Choi, T. & Gupta, J. A. Tunneling spectroscopy of ultrathin insulating films: CuN on Cu(100). *Appl. Phys. Lett.* **91**, 253106 (2007).
23. Repp, J., Meyer, G., Paavilainen, S., Olsson, F. E. & Persson, M. Scanning Tunneling Spectroscopy of Cl Vacancies in NaCl Films: Strong Electron-Phonon Coupling in Double-Barrier Tunneling Junctions. *Phys. Rev. Lett.* **95**, 225503 (2005).

24. Schintke, S. & Schneider, W.-D. Insulators at the ultrathin limit: electronic structure studied by scanning tunnelling microscopy and scanning tunnelling spectroscopy. *J. Phys.: Cond. Matter* **16**, 49–81 (2004).
25. Repp, J. *et al.* Controlling the Charge State of Individual Gold Adatoms. *Science* **305**, 493–495 (2004).
26. Repp, J., Meyer, G., Stojković, S. M., Gourdon, A. & Joachim, C. Molecules on Insulating Films: Scanning-Tunneling Microscopy Imaging of Individual Molecular Orbitals. *Phys. Rev. Lett.* **94**, 026803 (2005).
27. Rau, I. G. *et al.* Reaching the Magnetic Anisotropy Limit of a 3d Metal Atom. *Science* **344**, 988–992 (2014).

Methods:

Preparation of chlorine terminated Cu(100):

Cu(001) crystals were cleaned by repeated cycles of Argon sputtering and subsequent annealing at 550 °C. Cleanness of the crystals have been controlled using Low Energy Electron Diffraction (LEED) method and STM. The chlorine terminated Cu(100) substrate was prepared by thermal evaporation of anhydrous CuCl₂ powder from the quartz-crucible heated to 300 °C. Clean Cu(100) crystals are pre-heated to 150 °C prior to the deposition for 10 minutes, and kept at this temperature during the deposition and 10 minutes after the deposition⁹. The quality of the surface was verified with LEED and STM.

Acquisition of dz/dV maps:

dz/dV maps have been acquired in constant current mode, where consecutive topography images have been taken on the same area at different bias voltages in 10 mV intervals for checkerboard lattices and in 50 meV intervals for stripes lattices. The consecutive images have been subtracted, thus providing the height difference dz for each point of the topography images for a respective voltage difference. For qualitative details see Supplementary Note 1.

Numerical calculations:

We performed numerical calculations for a model Hamiltonian defined on two different geometries, for the checkerboard lattice and the second one the stripe lattice. In both situations the size of the lattice we took is exactly the same as in the experiment.

The calculations are performed in the tight binding approximation using a Hamiltonian with local orbitals in the form

$$H = \sum_{ij} t_{ij} c_j^{\dagger} c_i \quad (1)$$

where the parameters t_{ij} are the elements of the overlap matrix between states localized within the chlorine vacancies and defined as

$$t_{ij} = \langle \psi_i | H | \psi_j \rangle \quad (2)$$

and c_j^\dagger and c_i are creation and annihilation parameters at site j and i , respectively.

In our calculations, we use a value of -139 meV for first neighbour hopping term t_1 and a value of -38 meV for second neighbour hopping term t_2 . Furthermore, to simulate the potential well we use the edge potential of 38 meV for the checkerboard lattice and 80 meV, for the stripes lattice.

The effect of the hybridization with the metallic bath is taken into account by means of a self-energy parameter with finite imaginary part, that enters the Dyson equation of the Green function. For simplicity we assume the self-energy to be site-independent and diagonal, which allows to precisely reproduce the experimental features in a wide energy range. Green function is thus defined as follow

$$G(E) = (E - H - \Sigma)^{-1} \quad (3)$$

with self-energy term defined as

$$\Sigma = i\delta \quad (4)$$

where $\delta = 40$ meV.

Within the previous Green function, the density of states at the site i is given by

$$\rho_i(E) = \text{Im}(G_{ii}(E)) \quad (5)$$

The spatially resolved DOS is calculated assuming that the local states ψ_i is centered in \mathbf{r}_i have the form

$$\psi_i(\mathbf{r}) = N e^{-(\mathbf{r}-\mathbf{r}_i)^2/\sigma^2} \quad (6)$$

with $\sigma = 0.9a$, where a is the first neighbour vacancy-vacancy distance.

Supplementary information

Emergence of quasiparticle Bloch states in artificial crystals crafted atom-by-atom

J. Girovsky¹, J. L. Lado², F. E. Kalff¹, E. Fahrenfort¹, L.J.J.M. Peters¹, J. Fernández-Rossier^{2,3} and A. F. Otte¹

¹Department of Quantum Nanoscience, Kavli Institute of Nanoscience, Delft University of Technology, Lorentzweg 1, 2628 CJ Delft, The Netherlands.

²International Iberian Nanotechnology Laboratory (INL), Avenida Mestre José Veiga, 4715-310 Braga, Portugal.

³Departamento de Física Aplicada, Universidad de Alicante, San Vicente del Raspeig, 03690 Spain.

Supplementary Note 1

The arrangement of chlorine atoms in the checkerboard lattice is very sensitive to large tunnelling currents; a current exceeding $I > 1 \mu\text{A}$ frequently caused unintended displacement of the atoms. Such high currents are reached whilst acquiring differential conductance spectra (dI/dV), and causing the entire structure to collapse. In order to qualitatively extract the local density of states (DOS) in the checkerboard and stripes lattices, we used a method where, instead of acquiring (dI/dV) spectra, we recorded the tip-sample distance z as a function of applied bias voltage V . The time constant of the feedback-loop was much smaller ($t = 25 \mu\text{s}$) than the time set to measure a single data-point ($t \sim 1 \text{ s}$), ensuring thus that the tip had enough time to stabilize. In this mode the tunnelling current was kept constant at $I = 500 \text{ pA}$. In next step a numerical derivation of a z vs. V curve, i.e. the dz/dV curve, has been extracted (black, red and blue line in Supplementary Fig. 1). As the tunnel current I is exponentially proportional to the tip-sample distance z (see Supplementary Eq. 1),

$$I(z) = A V e^{-2 \frac{\sqrt{2m\phi}}{\hbar} z}, \quad (1)$$

where A is a constant, V the bias voltage, m the mass of the tunnelling electron, ϕ the height of the tunnelling barrier and \hbar the reduced Planck constant. Extracting z as a function of the tunnelling current and the applied bias voltage results in

$$z = \frac{\ln\left(\frac{I}{V}\right) - \ln(A)}{-2 \frac{\sqrt{2m\phi}}{\hbar}}. \quad (2)$$

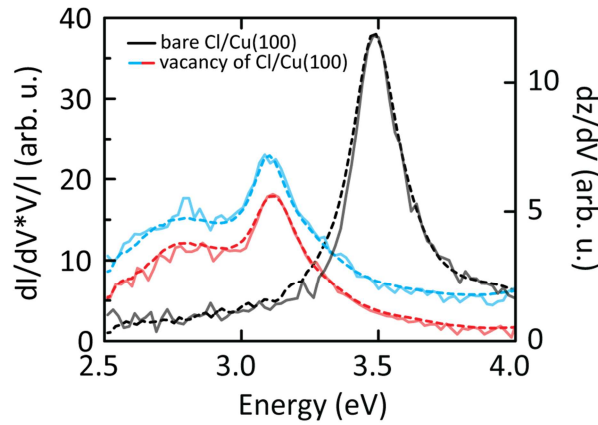
Derivation of the distance z to voltage gives

$$\frac{dz}{dV} \propto \frac{dI}{dV} \frac{V}{I}. \quad (3)$$

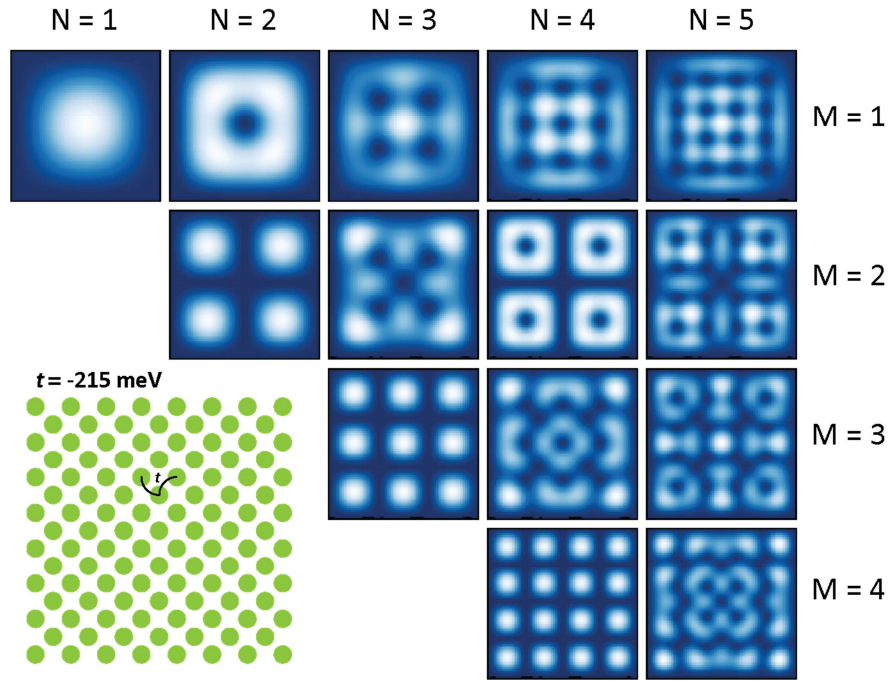
As can be seen from Supplementary Equation 3, the dz/dV is linearly proportional to the normalized differential conductance spectra ($dI/dV \cdot V/I$).

Supplementary Note 2

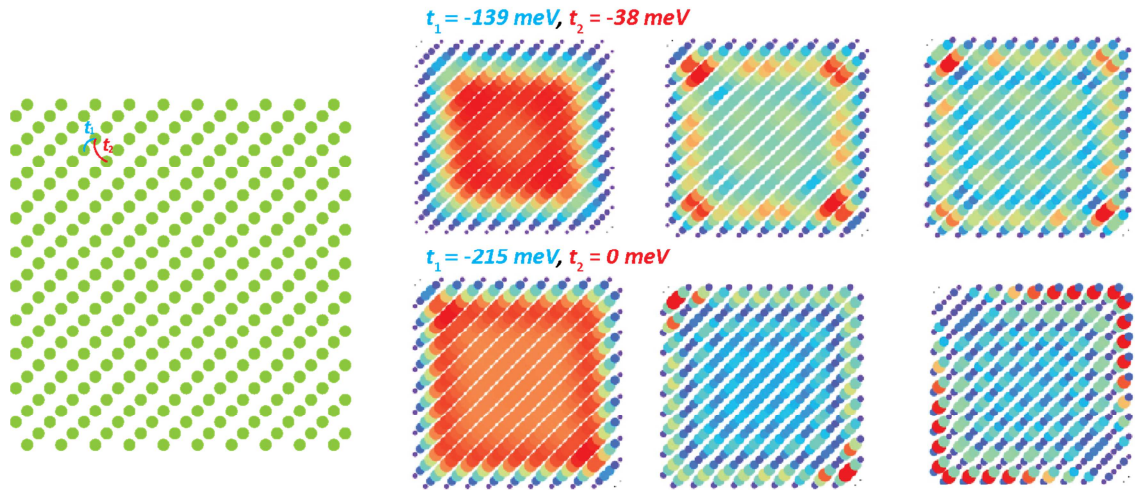
Theoretical calculations of artificial checkerboard lattice of size 8×8 using tight-binding approach with $t = -215$ meV without hybridization term are shown in Supplementary Figure 2, showing the individual modes. In two dimensions, the patterns are characterized by two vectors k_x and k_y , that are independent of each other. The vectors are defined as $k_x = N\pi/L$ and $k_y = M\pi/L$ where $N, M = (1, 2, 3, \dots, 8)$ are the mode numbers and L is the size of the lattice ($L = 8$ in our case). In order to get agreement with the experiment, a finite hybridization with the metal is needed. Furthermore, in the case of the stripes lattice, an additional next nearest neighbour hopping term is needed. In Supplementary Figure 3 We show calculations for the stripes lattice using the tight-binding model without hybridization term, (i) with nearest neighbour and next nearest neighbour hopping term and (ii) with nearest neighbour hopping term only. The best agreement with the experimental results is found when both terms are included.



Supplementary Figure 1 | Comparing dI/dV and $dI/dV * V/I$ spectra acquired on Cl/Cu(100). Dashed curves represent normalized $dI/dV * V/I$ spectra. The corresponding black, red and blue curves were taken at the same locations as the dashed ones, i.e. on the bare Cl/Cu(100) substrate (black) and on the vacancies within the stripes lattice (cyan and red).



Supplementary Figure 2 | Numerical calculations on checkerboard lattice using a tight-binding model. Standing wave patterns acquired for the numerical calculations with the hybridization with the environment term set to zero. The integers N and M denote number of modes for k_x and k_y axis.



Supplementary Figure 3 | Numerical calculations on stripes lattice using a tight-binding model. Standing wave pattern within the stripes lattice have been simulated using nearest neighbour and next nearest neighbour hopping terms (top row) or nearest neighbour hopping term only (bottom row). Experimental data are better reproduced using both the nearest and next-nearest hopping term.